# Targeted suppression of microRNA-33 in lesional macrophages using pH low-insertion peptides (pHLIP) improves atherosclerotic plaque regression

**Xinbo Zhang**
Yale University School of Medicine https://orcid.org/0000-0002-9184-5767
**Noemi Rotllan**
Yale University School of Medicine https://orcid.org/0000-0002-0587-8045
**Alberto Canfrán-Duque**
Yale University School of Medicine
**Jakub Toczek**
Yale University School of Medicine
**Anna Moshnikova**
The University of Rhode Island
**Shipra Malik**
University of Connecticut
**Nathan Price**
Yale University School of Medicine
**Elisa Araldi**
ETH Zurich https://orcid.org/0000-0002-6596-6784
**Wen Zhong**
Yale University School of Medicine
**Mehran Sadeghi**
Yale University School of Medicine
**Oleg Andreev**
The University of Rhode Island
**Raman Bahal**
University of Connecticut
**Yana Reshetnyak**
The University of Rhode Island
**Yajaira Suarez**
Yale University School of Medicine
**Carlos Fernandez-Hernando** ( carlos.fernandez@yale.edu )
Yale University School of Medicine

**Letter**

**Keywords:** pHLIP, microRNA-33, atherosclerosis, regression

**Posted Date:** October 29th, 2020

**DOI:** https://doi.org/10.21203/rs.3.rs-92252/v1

# Abstract

Hypoxia and tissue acidification occur in the macrophage-rich regions of advanced atherosclerotic lesions due to the higher oxygen demand of activated immune cells and insufficient oxygen supply. Our group and others originally identified microRNA-33 (miR-33) as critical regulator of cellular lipid homeostasis and lipoprotein metabolism controlling the development of atherosclerosis. Our prior work has demonstrated that pH Low-Insertion Peptides (pHLIP) can be used to direct miR-33 inhibitors to acidic microenvironments and protect against kidney fibrosis. Here we utilize anti-miR-33 conjugated pHLIP constructs to target macrophages located in atherosclerosis plaques. The inhibition of miR-33 using pHLIP-directed targeting increased collagen content and decreased lesional lipid accumulation within atherosclerotic plaques in a murine model of atherosclerosis regression. Single cell RNA sequencing analysis revealed higher expression of fibrotic genes (*Col2a1, Col3a1, Fn1, Dcn*, etc) and tissue inhibitor of metalloproteinase 3 (*Timp3*), and downregulation of matrix metallopeptidase 12 (*Mmp12*) in macrophages from atherosclerotic lesions targeted by pHLIP- anti-miR-33. These results suggest a potential application of pHLIP for treating advanced atherosclerosis via pharmacological inhibition of miR-33.


# Main

Atherosclerosis is well-known as a chronic inflammatory disease and disorder of lipid metabolism involving the retention of atheroprone lipoproteins and accumulation of monocyte-derived macrophages triggering maladaptive immune response and necrotic core formation.[1] The oxygen supply of vascular cells in atherosclerosis relies on the luminal blood or the adventitial vasa vasorum, and the distance to the deep layer of the intima exceeds the oxygen diffusion threshold resulting in local hypoxia[2, 3, 4, 5]. The uptake of modified lipoproteins by macrophages differentiated from recruited monocytes results in the accumulation of macrophage foam cells in the atherosclerotic lesions. Specifically, hypoxia strongly correlates with the macrophage foam cell clusters surrounding the plaque core[6]. The higher oxygen demand of activated immune cells and insufficient oxygen supply lead to severe hypoxia and tissue acidification in the macrophage-rich regions of atherosclerotic lesions[7, 8]. Notably, the acidic extracellular environment in macrophage foam cells impairs the expression of ATP-binding cassette transporter ABCA1, resulting in decreased cholesterol efflux and accelerated lipid accumulation[9].

Our group and others initially identified microRNA-33 (miR-33) as crucial regulator of cellular lipid homeostasis and lipoprotein metabolism, controlling downstream target genes including ABCA1 and ABCG1[10, 11, 12, 13, 14, 15, 16]. The benefits of miR-33 deficiency on atherosclerosis development are attributed to its protective effects in macrophages[12] Therapeutic inhibition of miR-33 in the mice and non-human primates raises plasma high density lipoprotein (HDL) levels and inhibits the progression of atherosclerosis by increasing HDL levels/functionality or enhancing cholesterol efflux through induction of ABCA1 and ABCG1 in macrophages[14, 15, 16, 17]. Notably, specific disruption of *Abca1* targeting by miR-33 is sufficient to mimic the effects of miR-33 deficiency on cholesterol efflux and atherogenesis[18].

However, long-term silencing of miR-33 increases circulating triglycerides levels and lipid accumulation in the liver through upregulation of genes involved in fatty acid synthesis when mice are fed a high-fat diet, indicating deleterious effects of moderate hepatic steatosis and hypertriglyceridemia[19]. Moreover, genetic models of miR-33 deficiency showed a strong predisposition to obesity and metabolic dysfunction[12, 13, 19, 20] Thus, specific targeting of miR-33 in the macrophages of atherosclerotic lesions could provide an effective therapeutic strategy for atherosclerosis that avoids the deleterious effects in other metabolic tissues.

pH-Low Insertion Peptides (pHLIP) are a novel class of water-soluble membrane molecules that target areas of high acidity at the surface of cells, which have been employed to deliver miRNA inhibitors to the acidic environment of tumors and the kidney[21, 22]. Given the hypoxia in macrophage foam cells and the acidic environment of the lipid core in atherosclerosis, we explore the utility of anti-miR-33 peptide nucleic acid (PNA) delivery vectors (anti-miR-33$^{pHLIP}$) for specific targeting of the macrophages in vascular lesions (Fig. 1a). Notably, near-infrared fluorescence imaging showed highly specific uptake of pHLIP variant 3 conjugated with fluorescent Alexa 750 (A750-Var3) in the aortic arch, an atherosclerotic prone area, of hypercholesterolemic mice. Other tissues characterized by the acidic microenvironment such as the kidney also accumulate the peptide. The targeting of VAR3 to atherosclerotic plaques was specific since a similar peptide with an altered amino acid sequence that prevents insertion across the membranes in acidic conditions (A546-5K-Var3) was unable to target vascular lesions (Fig. 1b). The targeting of A546-Var3 into the aortic arch occurred early (4 hours) and was sustained for 24 hours (**Supp** Fig. 1a and **b**). Imaging of whole organs indicated that uptake in the liver was diminished with the A546-Var3 compared to the A546-5K-Var3 mutant (**Supp** Fig. 1a and **b**), while similar fluorescent density was observed in histologic sections (**Supp** Fig. 1c). Both techniques demonstrated higher uptake of A546-Var3 in primary renal tubular cells (**Supp** Fig. 1c). The affinity of A750-Var3 to atherosclerotic aortic arch was confirmed by analyzing aortas in low-density lipoprotein receptor knockout (*Ldlr*$^{-/-}$) and WT mice injected with A750-Var3, A750-5K-Var3 or PBS (Fig. 1c). We further demonstrated the internalization of A750-Var3 in isolated macrophages from atherosclerotic aortas by flow cytometry. The results showed a significant uptake of A750-Var3 in macrophages (Lin$^{-}$CD11b$^{high}$F4/80$^{+}$Ly-6C$^{low}$) and less pronounced internalization in monocytes (Lin$^{-}$CD11b$^{high}$F4/80$^{-}$Ly-6C$^{high}$) from atherosclerotic plaques (Fig. 1d). These findings correlate with our previous studies showing a specific uptake of pHLIP in tumor associated macrophages.[23] Similar to the results observed *in vivo*, acidification of the media (pH = 6.2) promoted a marked increase of A546-Var3 uptake in mouse macrophages compared to macrophages cultured at a neutral pH (Fig. 2a). Assessment of fluorescently labeled constructs (A633-Var3) confirmed the high uptake by *in vivo* foam cells isolated from *Ldlr*$^{-/-}$ mice fed a WD for 3 months using both fluorescent microscopy and flow cytometry (Fig. 2b). Next, we tested whether the delivery of anti-miR-33$^{pHLIP}$ was able to enhance the expression of ABC transporters and reduce foam cell formation *in vivo*. We found that suppressing miR-33 in macrophages using anti-miR-33$^{pHLIP}$ resulted in significant reduction of neutral lipid accumulation compared to macrophages treated with a non-targeting antisense oligonucleotide conjugated with pHLIP (Src$^{pHLIP}$) (Fig. 2c, *quantified in right panel*). The marked reduction

in foamy macrophages correlated with an increase of ABCA1 expression in anti-miR-33$^{pHLIP}$ treated macrophages (Fig. 2d, *quantified in right panel*). Together, these results demonstrate that pHLIP is an effective and highly specific vehicle to target the expression of miRNAs in macrophages accumulated in atherosclerotic plaques.

We next assessed the efficacy of inhibiting miR-33 expression in lesional macrophages during the regression of atherosclerosis. To this end, *Ldlr*$^{-/-}$ mice were fed a Western diet (WD) for 3 months to establish atherosclerotic plaques, then switched to a chow diet (CD) and injected with Src$^{pHLIP}$ and anti-miR-33$^{pHLIP}$ (1 mg/Kg) weekly for one month (Fig. 3a). Consistent with previous studies, switching *Ldlr*$^{-/-}$ mice to CD resulted in a significant decrease of circulating total cholesterol (TC) and triglycerides (TG) level and increase in plasma HDL-C (**Supp** Fig. 2a). However, there was no difference between mice treated with anti-miR-33$^{pHLIP}$ and Src$^{pHLIP}$, suggesting that the hepatic delivery of anti-miR-33 using pHLIP was not sufficient to impact regulation of HDL biogenesis by miR-33 in the liver (**Supp** Fig. 2a). Similar lipoprotein profiles (**Supp** Fig. 2b), body weight (**Supp** Fig. 2c) and circulating leukocytes (**Supp** Fig. 3a) were observed in mice treated with anti-miR-33$^{pHLIP}$ and Src$^{pHLIP}$. Additionally, no changes in serum hepatotoxicity markers, aspartate aminotransferase (AST) and alanine aminotransferase (ALT), were found in mice treated with anti-miR-33$^{pHLIP}$ compared with Src$^{pHLIP}$-treated mice (**Supp** Fig. 3b).

We next sought to determine whether delivery of anti-miR-33 by pHLIP peptides could contribute to the regression of established atherosclerotic plaques. Consistent with our previous studies,[24] miR-33 antisense oligonucleotide treatment did not influence plaque size as compared with mice treated with Src$^{pHLIP}$ (Fig. 3b, *quantified in right panel*). However, we found that anti-miR-33$^{pHLIP}$ treatment promoted a significant decrease of lipid accumulation in atherosclerotic lesions, which correlated with higher expression of *Abca1* mRNA in the aorta (Fig. 3c and **d**). No differences in Abca1 expression was found in the liver of mice injected with anti-miR-33$^{pHLIP}$ and Src$^{pHLIP}$, suggesting that pHLIP direct the specific silencing of miR-33 into the arterial wall (**Supp Fig. 5)**. We further characterized the plaques by analyzing markers of inflammation and lesion stability. Quantification of macrophage content in the lesions by CD68$^{+}$ staining demonstrated a non-significant decrease in anti-miR-33$^{pHLIP}$ treated mice compared to controls (**Supp Fig. 5**). Notably, there was a significant increase in lesional collagen (Fig. 3e, *quantification right panel*) without any effect on smooth muscle cell content (**Supp Fig. 5)** in mice treated with anti-miR-33$^{pHLIP}$. Together, these results indicate that targeted inhibition of miR-33 in vascular lesions promotes macrophage cholesterol efflux and atherosclerotic plaque remodeling resulting in a more stable phenotype.

To assess the potential mechanisms by which anti-miR-33$^{pHLIP}$ regulates macrophage function and regression of atherosclerosis, we isolated live whole cells from enzyme-digested aortas of anti-miR-33$^{pHLIP}$- and Src$^{pHLIP}$-treated mice and performed single cell transcriptomics (Fig. 4a, **Supp Fig. 5**). A total of 7,771 Src$^{pHLIP}$ cells and 13,424 anti-miR-33$^{pHLIP}$ cells were obtained from atherosclerotic plaques in each group and run on the 10x Genomics platform. Unsupervised Seurat-based clustering identified 12 distinct cell clusters based on gene expression of established canonical markers including

monocytes/macrophages (Mono/Mac, Cluster 2, 10 and 11), endothelial cells (EC, Cluster 3), dendritic cells (DC, Cluster 8), vascular smooth muscle cells (VSMC, Cluster 0, 1 and 4), T cells (Cluster 5 and 7) and fibroblasts (Cluster 6 and 9) (Fig. 4a, **Supp Fig. 6**). Given the cellular delivery of anti-miR-33 by pHLIP into macrophages and monocytes in atherosclerotic lesions (Fig. 1d), we further analyzed the phenotype of these Mono/Mac populations during the regression of atherosclerosis (**Supp Fig. 6a** and **b**). Specific gene expression profiles differentiated 5 aortic monocyte and macrophage populations from the Mono/Mac clusters (Fig. 4b, **Supp Fig. 7a**). These included Trem2$^{high}$ Mac (Cluster 0: *Trem2, Cd9, Spp1, Lgals3*), F10$^{+}$ Mono (Cluster 2: *F10, Ccr2*, low *H2-Eb1*), Inflammatory Mac (Cluster 3: *Il1b, Cxcl2, Nfkbiz, S100a9, S100a8*) and Stem-like Mac (Cluster 4: *Top2a, Ube2c, Cenpf, Stmn1*) (**Supp Fig. 7b**). Interestingly, besides these well-established cell populations found in atherosclerotic lesions (Trem2$^{high}$ Mac, F10$^{+}$ Mono, Inflammatory Mac and Stem-like Mac),[25, 26] we observed one specific macrophage cluster (Cluster 1, herein referred to as "ECM$^{high}$ Mac") that expressed monocyte and macrophage genes (*Cd14, Cd68, Adgre1* and *Csf1r*) (**Supp Fig. 7a**) and was highly enriched for extracellular matrix (ECM)-associated genes, including *Col1a2, Col3a2, Col1a1, Fn1, Eln, Lum, Bgn* and *Dcn* (Fig. 4c, **Supp Fig. 7c**). The percentage of ECM$^{high}$ Mac were increased in the mice treated with anti-miR-33$^{pHLIP}$ as compared to Src$^{pHLIP}$ (Fig. 4d). This intriguing finding indicate that during the regression of atherosclerosis suppression of miR-33 in macrophages promotes a pro-fibrotic phenotype that favour plaque stabilization. Notably, the population of inflammatory macrophages (Cluster 3) characterized by the high expression of pro-inflammatory cytokines and chemokines was decreased, and the "stem-like macrophages" in cluster 4, enriched for cell cycle genes and highly proliferative, were increased in the mice treated with anti-miR-33$^{pHLIP}$ as compared to Src$^{pHLIP}$ (Fig. 4d). We next performed pathway enrichment analysis associated with changes in gene expression in Mono/Mac cells. Among all the pathways that were significantly altered in response to anti-miR-33$^{pHLIP}$ treatment, we found upregulated fibrosis, M2 polarization (IL-4 Signaling) and antigen presentation pathways (Fig. 4e). In addition to an increased signature with extracellular matrix (Fig. 4f), we also observed a decrease of inflammatory genes (*Cxcl2* and *Tnfsf9*) and an increase of antigen presentation genes (*H2-Eb1*, *H2-Aa* and *H2-Ab1*) in the mice treated with anti-miR-33$^{pHLIP}$ (Fig. 4g), indicating that anti-miR-33 treatment by pHLIP peptides induces macrophages towards a less inflammatory and more stable phenotype in the atherosclerotic lesions.

In conclusion, we demonstrated the remarkable selectivity of pHLIP peptides to target macrophages in atherosclerotic lesions based on their affinity for acidic microenvironments. The specific delivery of anti-miR-33 to atherosclerotic plaques using pHLIP peptides promotes a more stable phenotype by induction of ABCA1-mediated cholesterol efflux and extracellular matrix deposition. These findings highlight the therapeutic potential of anti-miR-33$^{pHLIP}$ constructs for the regression of atherosclerosis, while avoiding the potential deleterious effects in other organs. The pHLIP technology can also be applied to the selective delivery of other protective miRNAs to the macrophages from atherosclerotic plaques for the therapy of atherosclerosis-associated cardiovascular diseases. One of the most unique aspects of miRNAs is their ability to target many different mRNAs, which allows them exert both very nuanced and

extremely pronounced effects in different situations. However, this promiscuity has also raised important concerns for both research on and clinical applications, especially since the target preferences and impact of miRNAs can vary dramatically in different tissues and cell types. Considering the potential for disparate and possibly adverse effects in different organs, targeted delivery systems such as that described in this work may prove incredibly valuable for the development of safe and reliable miRNA-based therapies.

## Methods

# Animals

Wide-type (WT) and low-density lipoprotein receptor knockout (*Ldlr*$^{-/-}$) were obtained from The Jackson Laboratory. *Ldlr*$^{-/-}$ mice were fed a high-fat and high-cholesterol Western-type diet (WD, 40% fat and 1.25% cholesterol, #D12108, Research Diets, Inc., New Brunswick, NJ) for 1 or 3 months to induce atherosclerosis. Mice used in all experiments were sex and age matched, kept in individually ventilated cages in pathogen-free facility. All the experiments were approved by the Institutional Animal Care Use Committee of Yale University School of Medicine.

# Synthesis of PNA

The synthesis of antimiR-33 and scramble PNA was performed as reported previously [27, 28]. Boc-PNA regular monomers used for the synthesis were purchased from ASM Chemicals and Research (Germany). Solid phase synthesis of PNA was carried out on 4-methylbenzylhydramine (MBHA) resin and cysteine was conjugated on N-terminus of PNAs. After completion of synthesis, PNA was cleaved from the resin using cleavage cocktail (Trifluoromethanesulfonic acid: trifluoroacetic acid: dimethyl sulfide: m-cresol, 2:6:1:1) and precipitated using diethyl ether. Further purification of PNA was performed using reverse phase high performance liquid chromatography (RP-HPLC). Mass spectroscopy (matrix assisted laser desorption/ ionization time of flight, MALDI) was used to confirm the molecular weight and concentration of PNAs was determined using UV-spectroscopy.

# Synthesis and fluorescent labeling of pHLIP-PNA

pHLIP-PNA conjugations were performed as previously described.[22, 29] Briefly, Aldrithiol-2 (Millipore Sigma) was conjugated with pHLIP-Cys (ADDQNPWRAYLDLLFPTDTLLLDLLWCG, CS Bio) in dimethylformamide (DMF) at have a molar ratio of 1:1. The reaction mix was then mixed with 100 mM sodium phosphate and 150 mM NaCl buffer, pH 7.2 (saturated with argon), incubated at RT for 1 hour, purified by reverse-phase HPLC (Zorbax SB-C18 columns, 9.4 × 250 mm, 5 μm; Agilent Technologies, the gradient consisting of a binary solvent system using water and acetonitrile with 0.05% trifluoroacetic acid [TFA] for 20–70% over 40 minutes), lyophilized, and characterized by surface-enhanced laser desorption/ionization time-of-flight (SELDI-TOF) mass spectrometry. Subsequently, PNAs were added to pHLIP-Cys(Pys) in DMSO (molar ratio 1:3) in the presence of 0.1 M ammonium bicarbonate, pH 8.8 (saturated with argon), incubated overnight at 30 °C, purified by reverse-phase HPLC, lyophilized, and

characterized by SELDI-TOF mass spectrometry. pHLIP (ACDDQNPWRAYLDLLFPTDTLLLDLLWA) and K-pHLIP (ACKKQNPWRAYLKLLFPTKTLLL KLLW) were conjugated at the N-terminus with Alexa Fluor 546-, 633- and Alexa Fluor 750-maleimide (Life Technologies) in DMF at a ratio of 1:1 at room temperature for about 2 hours. Constructs were purified by reverse-phase HPLC, lyophilized, and characterized by SELDI-TOF mass spectrometry. The concentrations of the constructs were determined by their absorbance using the following molar extinction coefficients: $\varepsilon_{554}$ = 93,000 M/cm (for Alexa Fluor 546-pHLIPs), $\varepsilon_{633}$ = 159,000 M/cm (for Alexa Fluor 633-pHLIPs), and $\varepsilon_{753}$ = 290,000 M/cm (for Alexa Fluor 750-pHLIPs).

# Assessment of pHLIP delivery

To determine the specificity of pHLIP delivery, animals were injected intravenously with pHLIP-A750-Var3 or the non-inserting control peptide pHLIP-A750-5K-Var3 (4 nmol). Animals were sacrificed after 4, 12 and 24 hours, and uptake in different tissues was determined by near-infrared fluorescence imaging, performed on an IVIS Spectrum system (Caliper Life Science) with appropriate excitation (Ex) and emission (Em) filter sets (Ex/Em = 745/800 nm). For flow cytometry analysis, entire aortas (from the root to the iliac bifurcation) were harvested 4 hours after injection with pHLIP-A750-5K-Var3 or pHLIP-A750-Var3. The aortas were cut into small pieces and subjected to enzymatic digestion with 400 U/ml collagenase I, 125 U/ml collagenase XI, 60 U/ml DNAse I and 60 U/ml hyaluronidase (Sigma-Aldrich) for 1 h at 37ºC while shacking. Macrophages and monocytes were identified with the following antibodies (all from Biolegend): Lineage-PE (CD3, CD90.2 clone 53 – 2.1, CD19, Ly6G colne IA8, NK1.1 clone PK126, Ter119 clone Ter119, CD11c clone HL3), CD11b-PacificBlue clone M1/70, F4/80-APC (BM8) and Ly6-C-FITC (clone AL-21). Flow cytometry was performed using a BD LSRII (BD Biosciences), and data were analyzed using FlowJo software v8.7 (Tree Star, Inc.).

# Anti-miR-33$^{pHLIP}$ treatment

*Ldlr* $^{-/-}$ mice were fed a WD for 3 months to induce atherosclerosis and then transferred to chow diet (CD) for 1 month. anti-miR-33$^{pHLIP}$ and Src$^{pHLIP}$ constructs were administered by intravenous injection at a dose of 1 mg/kg body weight in PBS with 5% DMSO. Injections were performed once every week (totally 5 times) during CD feeding before harvest. The mice fed with a WD for 3 months were harvested as Baseline for atherosclerosis analysis.

# Plasma lipids, lipoprotein profile and leukocytes analysis

After 3-month WD and 1-month CD feeding, mice were fasted for 12–14 h before blood samples were collected by retro-orbital venous plexus puncture. Plasma was separated by centrifugation and stored at -80 °C until analysis. Plasma total cholesterol (TC), high density lipoprotein-cholesterol (HDL-C) and triglyceride (TG) concentrations were determined by standard enzymatic methods (Wako Chemicals, USA). Plasma cholesterol fractions (VLDL, IDL/LDL and HDL) were detected by fast-performance liquid chromatography (FPLC) gel filtration on Superose 6 HR 10/30 size-exclusion column (Pharmacia) as described previously.[30] White blood cells (WBC) counting in circulation was determined from EDTA-anticoagulated blood using a hemocytometer (Hemavet Counter HV950FS). Circulating aspartate

aminotransferase (AST) and alanine aminotransferase (ALT) were analyzed using commercial enzymatic assays.

# Histology and morphometric analysis

Following anesthesia (100 mg/kg ketamine; 10 mg/kg xylazine), thoracic cavity was exposed immediately and *in situ* perfusion fixation through the left cardiac ventricle was performed by thorough perfusion with PBS and 4% paraformaldehyde (PFA). Subsequently, hearts and aortas were harvested and fixed in 10% formaldehyde solution overnight. Hearts were embedded in OCT after dehydration with 30% sucrose and serial sections were cut at 6 µm thickness using a cryostat. Every third slide from the serial sections was stained with haematoxylin and eosin (H&E) and each consecutive slide was stained with oil red O (ORO) for quantification of lesion area. Aortic lesion size of each animal was obtained by averaging the lesion areas in four sections from the same mouse. Collagen content was assessed by Picro Sirus Red staining of consecutive slides from serial sections and quantified as a percentage of the total plaque area.

# Immunofluorescence staining

The atherosclerotic sections were fixed with 4% PFA and incubated overnight with primary antibodies for CD68 (Serotec; #MCA1957) and Actin, α-smooth muscle-Cy3 (Sigma, #C6198) after blocking with blocker buffer (5% Donkey Serum, 0.5% BSA, 0.3% Triton X-100 in PBS) for 1 hour at RT, followed by incubation with Alexa Fluor secondary antibody (Invitrogen, Carlsbad, CA) for 1 hour at RT. The stained sections were captured using a Carl Zeiss scanning microscope Axiovert 200M imaging system and images were digitized under constant exposure time, gain, and offset. Results are expressed as the percent of the total plaque area stained measured with the Image J software (ImageJ version 1.51, Yale software library, Yale University).

# Aortic cells isolation from atherosclerotic lesions

To obtain the whole cells in the atherosclerotic lesions, the aorta was digested (from the root to the diaphragm) with 1 mg/ml Collagenase A (Roche, Cat 11088785103) for 7 min at 37 °C to remove the adventitia under microscope. Aortic tissue was cut into small pieces and subjected to enzymatic digestion with 1.5 mg/ml Collagenase A and 0.5 mg/ml Elastase (Worthington, Cat LS006365) for 40 min at 37 °C while shaking. The digested aortas were passed through a 70 µm Cell Strainer to obtain single cell suspensions followed by incubation of 10 minutes at 4 °C with 10 µg/ml of purified rat anti-mouse FcgRII/III (Biolegend) to block non-specific binding of antibodies to Fc Receptors. Total cell viability was obtained using live/dead viability dye eFluor 450 (Thermo Fisher Scientific). Viable cells were sorted by FACS Aria III (BD Biosciences) and immediately processed for single-cell RNA-seq.

# Droplet-based scRNA-seq library construction and sequencing

The sorted viable cells were encapsulated into droplets and processed following manufacturer's specifications using 10X Genomics GemCode Technology. Equal numbers of cells per sample were

loaded on a 10x Genomics Chromium controller instrument to generate single-cell Gel Beads in emulsion (GEMs) at Yale Center for Genome Analysis. Lysis and barcoded reverse transcription of polyadenylated mRNA from single cells were performed inside each GEM followed by cDNA generation using the Single Cell 3' Reagent Kits v3 (10X Genomics). Libraries were sequenced on an Illumina NovaSeq 6000 as 2 × 100 paired-end reads.

# Single cell RNA-seq data analysis

Sample demultiplexing, aligning reads to the mouse genome (mouse UCSC mm10 reference genome) with STAR and unique molecular identifier (UMI) processing were processed using CellRanger software (version 4.0.0) as previously described.[31] Low quality cells, doublets and potentially dead cells were filtered based on the percentage of mitochondrial genes and number of genes and UMIs expressed in each cell. After filtering we identified 7,771 $Src^{pHLIP}$ cells (a mean of 32,589 reads per cell, and a median 2,072 genes per cell) and 13,424 anti-miR-$33^{pHLIP}$ cells (a mean of 18,886 reads per cell, and a median 1,722 genes per cell) for downstream analysis. Data clustering was performed using Seurat R package (Version 3.0) with filtered genes by barcode expression matrices as inputs.[32] Highly variable genes (HVGs) were calculated using Seurat function FindVariableFeatures and used for downstream clustering analysis. Principal component analysis (PCA) was performed with RunPCA function (Seurat) using HVGs for dimensionality reduction and the number of significant principle components was calculated using JackStraw function. We applied the RunUMAP function to significant principal components (PCs) identified by JackStraw analysis and presented data in two-dimensional coordinates through uniform manifold approximation and projection (UMAP) generated by R package ggplot2. Clustering was done through FindClusters function using 30 significant PCs with a resolution of 0.3. Significantly differentially expressed genes in a cluster were analyzed using Seurat function FindAllMarkers, which were expressed in more than 25% of cells with at least 0.25-fold difference and reach statistical significance of an adjusted $p < 0.05$ as determined by the Wilcox test. Ingenuity Pathway Analysis (Ingenuity Systems QIAGEN, Content version: 47547484, 2019, Redwood City, CA, USA) was used to carry out analyses for pathway with differentially-expressed genes across samples.

# In vivo foam cell formation

*In vivo* foam cell formation was performed as previously described.[33] Briefly, $Ldlr^{-/-}$ mice were fed a WD for 3 months to establish atherosclerotic plaques, then switched to a chow diet (CD) and injected with $Src^{pHLIP}$ and anti-miR-$33^{pHLIP}$ (1 mg/Kg) weekly for one month. Peritoneal cells were collected from the peritoneal cavity 4 days after i.p. administration of 3% thioglycollate medium and allowed to adhere for 30 min. After removing non-adherent cells, the adherent macrophages were fixed by 4% PFA in PBS for 1 h and stained for 30 min with 0.3% Oil-Red O solution in 60% isopropanol. The mean area of Oil Red O-stained region per cell were quantified with 200 representative cells using Image J software from the NIH.

# Western blot analysis

*In vivo* foam cells were lysed in ice-cold buffer containing 50 mM Tris-HCl, pH 7.4, 0.1 mM EDTA, 0.1 mM EGTA, 1% NP-40, 0.1% sodium deoxycholate, 0.1% SDS, 100 mM NaCl, 10 mM NaF, 1 mM sodium pyrophosphate, 1 mM sodium orthovanadate, 1 mM Pefabloc, and 2 mg/ml protease inhibitor cocktail (Roche Diagnostics Corp). Protein concentrations were determined using the DC Protein assay kit (Bio-Rad Laboratories). Cell lysates containing 50 µg of protein were analyzed by SDS-PAGE and immunoblotting. Primary antibodies used include the following: anti-ABCA1 (Abcam, ab18180), anti-ABCG1 (Novus Biologicals, NB400-132) and anti-HSP90 (BD Biosciences, #610419). Secondary antibodies were fluorescence-labeled antibodies and bands were visualized using the Odyssey Infrared Imaging System (LI-COR Biotechnology).

# qPCR analysis

Total RNA from cells was isolated using TRIzol reagent. One microgram of total RNA was reverse-transcribed using the iScript RT Supermix (Bio-Rad, Hercules, CA, USA), following the manufacturer's protocol. Quantitative real-time PCR was performed in triplicate using iQ SYBR green Supermix (Bio-Rad) on a Real-Time Detection System (BioRad). The mRNA level was normalized to GAPDH as a housekeeping gene. Real-time PCR was conducted with gene expression levels with oligonucleotides specific for each of the genes.

# Flow cytometry

Blood was collected by retro-orbital puncture in heparinized micro-hematocrit capillary tubes. Erythrocytes were lysed with ACK lysis buffer (155 mM Ammonium Chloride, 10 mM Potassium Bicarbonate, 0.01 mM EDTA, pH 7.4). WBC were resuspended in 3% FBS in PBS, blocked with 2 µg/ml of FcgRII/III, then stained with a cocktail of antibodies. Monocytes were identified as CD115$^{hi}$ and subsets as Ly6-C$^{hi}$ and Ly6-C$^{lo}$; neutrophils were identified as CD115$^{lo}$Ly6-C$^{hi}$Ly6-G$^{hi}$. The following antibodies were used (all from BioLegend): FITC-Ly6-C (AL-21), PE-CD115 (AFS98), APC-Ly6-G (1A8). Flow cytometry was performed using a BD LSRII (BD Biosciences), and data were analyzed using FlowJo software v8.7 (Tree Star, Inc.).

# Statistical analysis

All data are expressed as mean ± s.e.m. Statistical differences were calculated with either unpaired two-sided Student's t-test or one-way analysis of variance (ANOVA, followed by the Bonferroni post-test). A value of $P \leq 0.05$ was considered statistically significant. Data analysis was performed using GraphPad Prism Software Version 7.0 (GraphPad, San Diego, CA).

## Declarations

# COMPETING FINANCIAL INTEREST

O.A.A. and Y.K.R. are founders of pHLIP, Inc. They have shares in the company, but the company did not fund any part of the work reported in this paper, which was carried out in their academic laboratories.

# AUTHOR CONTRIBUTIONS

CF-H and XZ conceived and designed the study and wrote the manuscript. XZ, NR, ACD, JD, AM, SM, EA, OA, YR and WZ performed experiments and analyzed data. NP, MS, OA, RB, YR, YS and CFH assisted with experimental design and data interpretation.

# ACKNOWLEDGEMENTS

This work was supported by grants from the National Institutes of Health (R35HL135820 to CF-H; R01HL105945 and R01HL135012 to YS and 1K01DK120794 to NP), the American Heart Association (16EIA27550005 to CF-H and 17SDG33110002 to NR).

## References

1. Tabas I, Bornfeldt KE. Macrophage Phenotype and Function in Different Stages of Atherosclerosis. *Circ Res* 2016, **118**(4): 653–667.
2. Levin M, Leppanen O, Evaldsson M, Wiklund O, Bondjers G, Bjornheden T. Mapping of ATP, glucose, glycogen, and lactate concentrations within the arterial wall. *Arterioscler Thromb Vasc Biol* 2003, **23**(10): 1801–1807.
3. Parathath S, Mick SL, Feig JE, Joaquin V, Grauer L, Habiel DM, *et al.* Hypoxia is present in murine atherosclerotic plaques and has multiple adverse effects on macrophage lipid metabolism. *Circ Res* 2011, **109**(10): 1141–1152.
4. Silvola JM, Saraste A, Forsback S, Laine VJ, Saukko P, Heinonen SE, *et al.* Detection of hypoxia by [18F]EF5 in atherosclerotic plaques in mice. *Arterioscler Thromb Vasc Biol* 2011, **31**(5): 1011–1015.
5. van der Valk FM, Sluimer JC, Voo SA, Verberne HJ, Nederveen AJ, Windhorst AD, *et al.* In Vivo Imaging of Hypoxia in Atherosclerotic Plaques in Humans. *JACC Cardiovasc Imaging* 2015, **8**(11): 1340–1341.
6. Sluimer JC, Gasc JM, van Wanroij JL, Kisters N, Groeneweg M, Sollewijn Gelpke MD, *et al.* Hypoxia, hypoxia-inducible transcription factor, and macrophages in human atherosclerotic plaques are correlated with intraplaque angiogenesis. *J Am Coll Cardiol* 2008, **51**(13): 1258–1265.
7. Khan T, Soller B, Naghavi M, Casscells W. Tissue pH determination for the detection of metabolically active, inflamed vulnerable plaques using near-infrared spectroscopy: an in-vitro feasibility study. *Cardiology* 2005, **103**(1): 10–16.
8. Naghavi M, John R, Naguib S, Siadaty MS, Grasu R, Kurian KC, *et al.* pH Heterogeneity of human and rabbit atherosclerotic plaques; a new insight into detection of vulnerable plaque. *Atherosclerosis* 2002, **164**(1): 27–35.
9. Lee-Rueckert M, Lappalainen J, Leinonen H, Pihlajamaa T, Jauhiainen M, Kovanen PT. Acidic extracellular environments strongly impair ABCA1-mediated cholesterol efflux from human macrophage foam cells. *Arterioscler Thromb Vasc Biol* 2010, **30**(9): 1766–1772.

10. Horie T, Ono K, Horiguchi M, Nishi H, Nakamura T, Nagao K, *et al.* MicroRNA-33 encoded by an intron of sterol regulatory element-binding protein 2 (Srebp2) regulates HDL in vivo. *Proc Natl Acad Sci U S A* 2010, **107**(40): 17321–17326.
11. Marquart TJ, Allen RM, Ory DS, Baldan A. miR-33 links SREBP-2 induction to repression of sterol transporters. *Proc Natl Acad Sci U S A* 2010, **107**(27): 12228–12232.
12. Price NL, Rotllan N, Canfran-Duque A, Zhang X, Pati P, Arias N, *et al.* Genetic Dissection of the Impact of miR-33a and miR-33b during the Progression of Atherosclerosis. *Cell Rep* 2017, **21**(5): 1317–1330.
13. Price NL, Singh AK, Rotllan N, Goedeke L, Wing A, Canfran-Duque A, *et al.* Genetic Ablation of miR-33 Increases Food Intake, Enhances Adipose Tissue Expansion, and Promotes Obesity and Insulin Resistance. *Cell Rep* 2018, **22**(8): 2133–2145.
14. Rayner KJ, Esau CC, Hussain FN, McDaniel AL, Marshall SM, van Gils JM, *et al.* Inhibition of miR-33a/b in non-human primates raises plasma HDL and lowers VLDL triglycerides. *Nature* 2011, **478**(7369): 404–407.
15. Rayner KJ, Suarez Y, Davalos A, Parathath S, Fitzgerald ML, Tamehiro N, *et al.* MiR-33 contributes to the regulation of cholesterol homeostasis. *Science* 2010, **328**(5985): 1570–1573.
16. Rotllan N, Ramirez CM, Aryal B, Esau CC, Fernandez-Hernando C. Therapeutic silencing of microRNA-33 inhibits the progression of atherosclerosis in Ldlr-/- mice–brief report. *Arterioscler Thromb Vasc Biol* 2013, **33**(8): 1973–1977.
17. Horie T, Baba O, Kuwabara Y, Chujo Y, Watanabe S, Kinoshita M, *et al.* MicroRNA-33 deficiency reduces the progression of atherosclerotic plaque in ApoE-/- mice. *J Am Heart Assoc* 2012, **1**(6): e003376.
18. Price NL, Rotllan N, Zhang X, Canfran-Duque A, Nottoli T, Suarez Y, *et al.* Specific Disruption of Abca1 Targeting Largely Mimics the Effects of miR-33 Knockout on Macrophage Cholesterol Efflux and Atherosclerotic Plaque Development. *Circ Res* 2019, **124**(6): 874–880.
19. Goedeke L, Salerno A, Ramirez CM, Guo L, Allen RM, Yin X, *et al.* Long-term therapeutic silencing of miR-33 increases circulating triglyceride levels and hepatic lipid accumulation in mice. *EMBO Mol Med* 2014, **6**(9): 1133–1141.
20. Horie T, Nishino T, Baba O, Kuwabara Y, Nakao T, Nishiga M, *et al.* MicroRNA-33 regulates sterol regulatory element-binding protein 1 expression in mice. *Nat Commun* 2013, **4**: 2883.
21. Cheng CJ, Bahal R, Babar IA, Pincus Z, Barrera F, Liu C, *et al.* MicroRNA silencing for cancer therapy targeted to the tumour microenvironment. *Nature* 2015, **518**(7537): 107–110.
22. Price NL, Miguel V, Ding W, Singh AK, Malik S, Rotllan N, *et al.* Genetic deficiency or pharmacological inhibition of miR-33 protects from kidney fibrosis. *JCI Insight* 2019, **4**(22).
23. Sahraei M, Chaube B, Liu Y, Sun J, Kaplan A, Price NL, *et al.* Suppressing miR-21 activity in tumor-associated macrophages promotes an antitumor immune response. *J Clin Invest* 2019, **129**(12): 5518–5536.

24. Distel E, Barrett TJ, Chung K, Girgis NM, Parathath S, Essau CC, *et al.* miR33 inhibition overcomes deleterious effects of diabetes mellitus on atherosclerosis plaque regression in mice. *Circ Res* 2014, **115**(9): 759–769.
25. Lin JD, Nishi H, Poles J, Niu X, McCauley C, Rahman K, *et al.* Single-cell analysis of fate-mapped macrophages reveals heterogeneity, including stem-like properties, during atherosclerosis progression and regression. *JCI Insight* 2019, **4**(4).
26. Cochain C, Vafadarnejad E, Arampatzi P, Pelisek J, Winkels H, Ley K, *et al.* Single-Cell RNA-Seq Reveals the Transcriptional Landscape and Heterogeneity of Aortic Macrophages in Murine Atherosclerosis. *Circ Res* 2018, **122**(12): 1661–1674.
27. Christensen L, Fitzpatrick R, Gildea B, Petersen KH, Hansen HF, Koch T, *et al.* Solid-phase synthesis of peptide nucleic acids. *J Pept Sci* 1995, **1**(3): 175–183.
28. Malik S, Lim J, Slack FJ, Braddock DT, Bahal R. Next generation miRNA inhibition using short anti-seed PNAs encapsulated in PLGA nanoparticles. *J Control Release* 2020, **327**: 406–419.
29. Andreev OA, Dupuy AD, Segala M, Sandugu S, Serra DA, Chichester CO, *et al.* Mechanism and uses of a membrane peptide that targets tumors and other acidic tissues in vivo. *Proc Natl Acad Sci U S A* 2007, **104**(19): 7893–7898.
30. Ramirez CM, Zhang X, Bandyopadhyay C, Rotllan N, Sugiyama MG, Aryal B, *et al.* Caveolin-1 Regulates Atherogenesis by Attenuating Low-Density Lipoprotein Transcytosis and Vascular Inflammation Independently of Endothelial Nitric Oxide Synthase Activation. *Circulation* 2019, **140**(3): 225–239.
31. Zheng GX, Terry JM, Belgrader P, Ryvkin P, Bent ZW, Wilson R, *et al.* Massively parallel digital transcriptional profiling of single cells. *Nat Commun* 2017, **8**: 14049.
32. Satija R, Farrell JA, Gennert D, Schier AF, Regev A. Spatial reconstruction of single-cell gene expression data. *Nat Biotechnol* 2015, **33**(5): 495–502.
33. Das R, Ganapathy S, Mahabeleshwar GH, Drumm C, Febbraio M, Jain MK, *et al.* Macrophage gene expression and foam cell formation are regulated by plasminogen. *Circulation* 2013, **127**(11): 1209–1218, e1201-1216.

# Figures

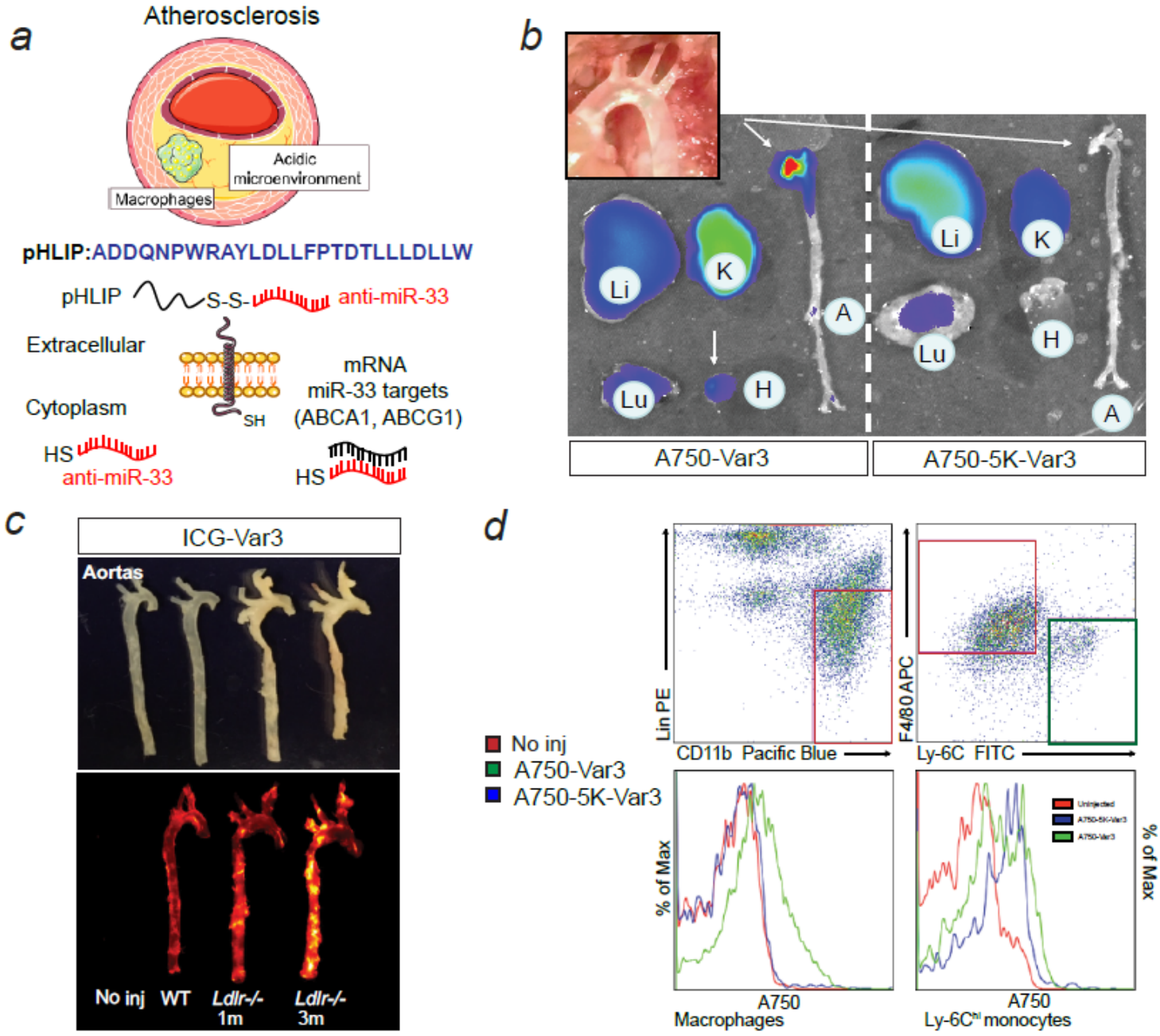


## Figure 1

pH low inducible peptides promote delivery of miR-33 inhibitors to the macrophages in atherosclerotic plaques. a, Generation of anti-miR-33 PNA-conjugated pH low insertion peptides (pHLIP) variant 3 capable of delivering miR-33 inhibitors to acidic microenvironments. b, Representative images of tissues from low density lipoprotein receptor knockout (Ldlr-/-) mice injected with fluorescently labeled targeted (A750-Var3) or non-inserting control (A750-5K-Var3) constructs. Ldlr-/- mice were fed a western diet (WD) for 3 months to induce atherosclerosis and tissues were harvested 4 hours post injection of constructs. c, Representative images of aortas from WT or Ldlr-/- mice injected with PBS, A750-5K-Var3 or A750-Var3 constructs. Tissues were harvested 4 hours post injection. d, Representative flow cytometry histograms

showing fluorescence intensities in macrophages and monocytes isolated from atherosclerotic lesions of mice injected with PBS, A750-5K-Var3 or A750-Var3 constructs.

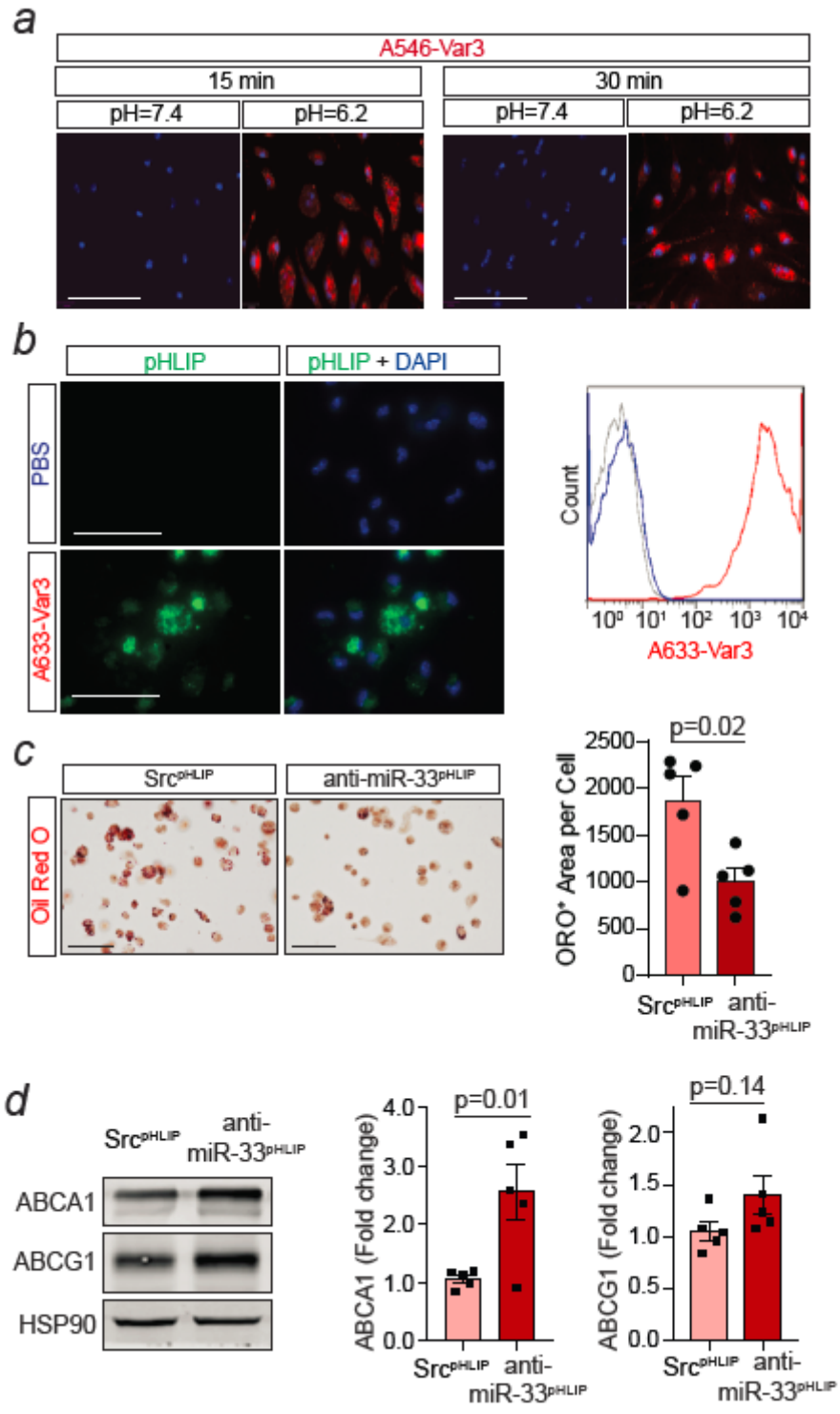


## Figure 2

Selective targeting of miR-33 by pHLIP peptides attenuates in vivo foam cell formation through induction of ABCA1. a, Representative confocal images of peritoneal macrophages incubated with fluorescently labeled pHLIP variant 3 constructs (A546-Var3). b, Representative images and flow cytometry histograms

of in vivo foam cells from mice injected with PBS and fluorescently labeled pHLIP variant 3 constructs (A633-Var3). c, Representative Oil-red O (ORO) staining of in vivo foam cells from mice injected with anti-miR-33 peptide nucleic acid delivery vector (anti-miR-33pHLIP) or scrambled control (SrcpHLIP). Quantification of lipid accumulation are shown in the right panel. Data were analyzed by an unpaired two-sided Student's t-test (n= 5 per group). d, Representative Western blot analysis of ABCA1 and ABCG1 in in vivo foam cells isolated from mice injected with anti-miR-33pHLIP or SrcpHLIP. Quantification are shown in the right panel. Data were analyzed by an unpaired two-sided Student's t-test (n= 5 per group). Quantification represents the mean ± s.e.m. Scale bar: 100 μm.

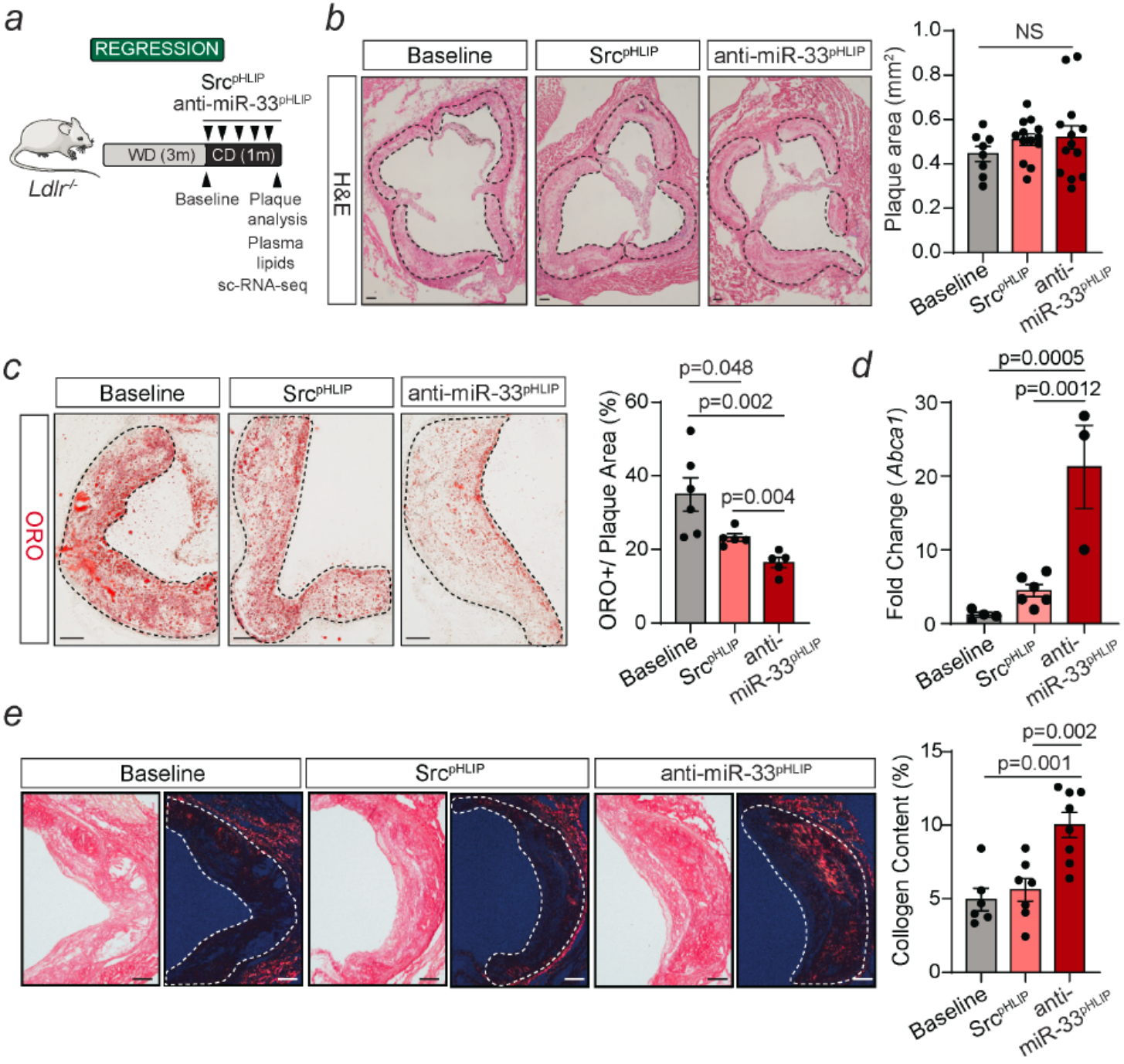


**Figure 3**

Targeted silencing of miR-33 improves regression of atherosclerosis. a, Experimental protocol for atherosclerosis regression. Low density lipoprotein receptor knockout (Ldlr-/-) mice were placed on a western diet (WD) for 3 months, and then switched to a chow diet and received anti-miR-33 peptide nucleic acid delivery vector (anti-miR-33pHLIP) or scrambled control (SrcpHLIP) at a dose of 1 mg/kg body weight every week for a total of 5 injections. b, Representative histological analysis of cross sections of the aortic root stained with hematoxylin and eosin (H&E) of Ldlr-/- mice injected with anti-miR-33pHLIP or SrcpHLIP vectors. Quantification of plaque size are shown in the right panel. Data were analyzed by one-way ANOVA with Bonferroni correction for multiple comparisons (n=12-13 per group). c, Representative Oil-red O (ORO) staining of cross sections of the aortic root from Ldlr-/- mice injected with anti-miR-33pHLIP or SrcpHLIP vectors. Quantification of lipid accumulation are shown in the right panel. Data were analyzed by one-way ANOVA with Bonferroni correction for multiple comparisons (n= 4-5 per group). d, qRT-PCR analysis of Abca1 mRNA expression in atherosclerotic aortas from Ldlr-/- mice injected with anti-miR-33pHLIP or SrcpHLIP vectors. Data were analyzed by one-way ANOVA with Bonferroni correction for multiple comparisons (n= 3-6 per group). e, Representative images of Picrosirus red staining of collagen in cross sections of the aortic root from Ldlr-/- mice injected with anti-miR-33pHLIP or SrcpHLIP vectors. Quantification of collagen content in atherosclerotic lesions are shown in the right panel. Data were analyzed by one-way ANOVA with Bonferroni correction for multiple comparisons (n= 6-8 per group). Quantification represents the mean ± s.e.m. Scale bar: 100 μm. NS, no significance.

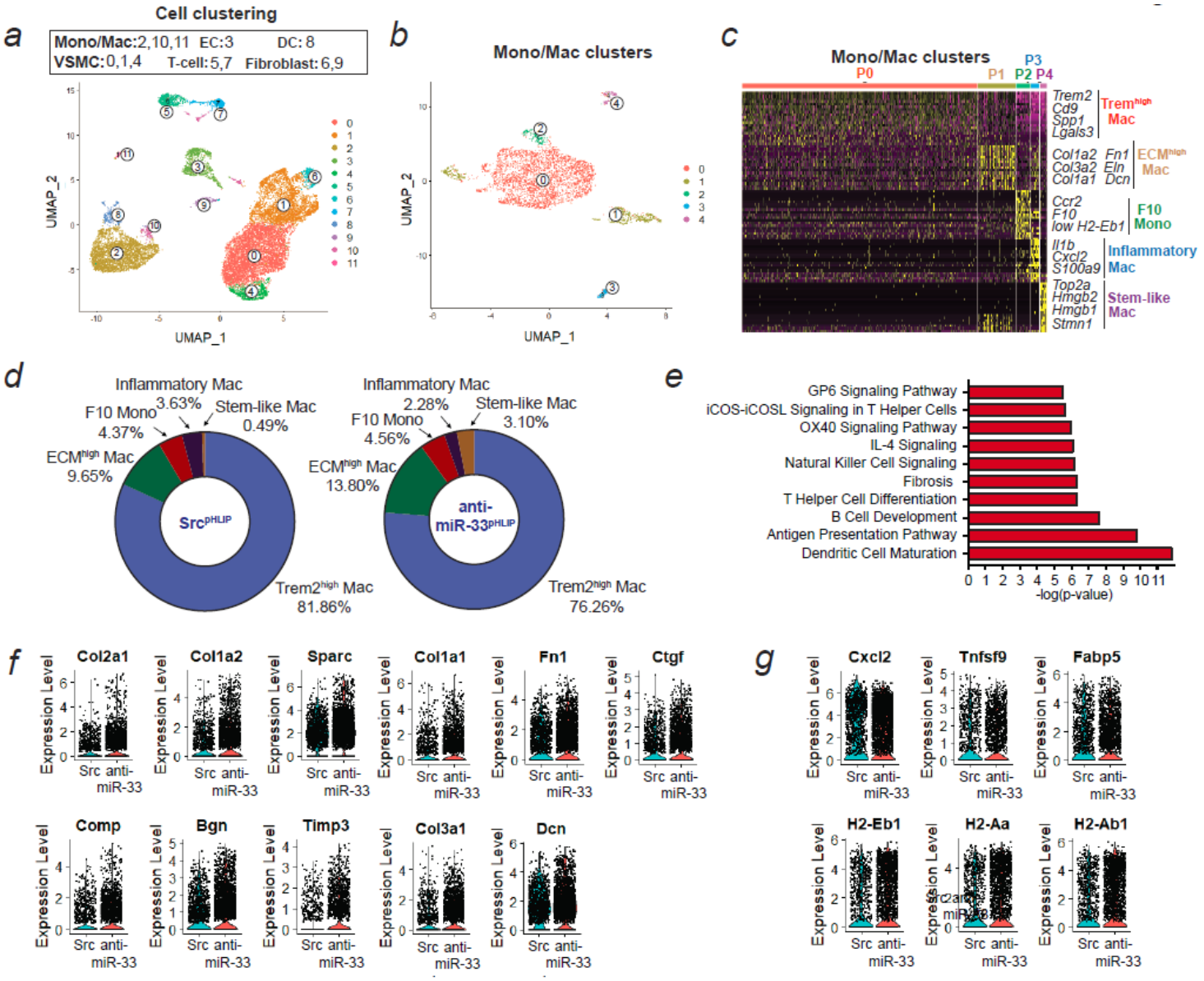


## Figure 4

Single cell RNA-Seq analysis reveals increased gene expression of extracellular matrix (ECM) in macrophages isolated from anti-miR-33pHLIP treated mice. a, Uniform manifold approximation and projection (UMAP) representation of aligned gene expression data in single cells extracted from atherosclerotic plaques of anti-miR-33pHLIP and SrcpHLIP-treated mice. UMAP dimensionality reduction analysis identified 12 major clusters. b, UMAP representation of aligned gene expression data in monocytes and macrophages (Mono/Mac) cluster extracted from atherosclerotic plaques. c, Heatmap of the 20 most upregulated genes in each cluster defined in b and selected enriched genes used for biological identification of each cluster. d, Proportions of defined Mono/Mac populations extracted from the atherosclerotic aortas of anti-miR-33pHLIP and SrcpHLIP-treated mice. e, Pathway enrichment of differentially expressed genes expressed as the log[−P] analyzed by Ingenuity Pathway Analysis. f, Violin plots of the top differentially expressed genes showing statistically significant upregulation of ECM in Mono/Mac population from anti-miR-33pHLIP-treated mice. g, Violin plots of the top differentially

expressed genes showing less inflammatory and higher antigen presentation genes in Mono/Mac population from anti-miR-33pHLIP-treated mice.

## Supplementary Files

This is a list of supplementary files associated with this preprint. Click to download.

- SUPPLEMENTALINFORMATION.pdf